Finite element homogenization technique for the characterization of d15 shear piezoelectric macro-fibre composites

Marcelo Areias Trindade, Ayech Benjeddou

Finite element homogenization technique for the characterization of d_{15} shear piezoelectric macro-fibre composites

M A Trindade[1] **and A Benjeddou**[2]

[1] Department of Mechanical Engineering, São Carlos School of Engineering,
University of São Paulo, Avenida Trabalhador São-Carlense, 400, São Carlos-SP, 13566-590,
Brazil
[2] Institut Supérieur de Mécanique de Paris, LISMMA/Structures, 3 rue Fernand Hainault,
93407 Saint Ouen, France

E-mail: trindade@sc.usp.br and benjeddou@supmeca.fr

Abstract
A finite element homogenization method for a shear actuated d_{15} macro-fibre composite (MFC) made of seven layers (Kapton, acrylic, electrode, piezoceramic fibre and epoxy composite, electrode, acrylic, Kapton) is proposed and used for the characterization of its effective material properties. The methodology is first validated for the MFC active layer only, made of piezoceramic fibre and epoxy, through comparison with previously published analytical results. Then, the methodology is applied to the seven-layer MFC. It is shown that the packaging reduces significantly the shear stiffness of the piezoceramic material and, thus, leads to significantly smaller effective electromechanical coupling coefficient k_{15} and piezoelectric stress constant e_{15} when compared to the piezoceramic fibre properties. However, it is found that the piezoelectric charge constant d_{15} is less affected by the softer layers required by the MFC packaging.

1. Introduction

Recent applications of piezoelectric sensors and actuators require conformability and packaging standards not found in monolithic piezoceramic patches [1]. The so-called macro-fibre composites (MFCs) have become very popular since they combine the conformability of epoxy matrix composites and the electromechanical energy density of piezoceramic materials [2]. The concept is based on the piezoelectric fibre composites (PFCs) proposed before [3] that used extruded piezoceramic fibres (circular cross-section) embedded in an epoxy-based resin matrix and covered by copper electrodes and protective Kapton and/or acrylic layers. However, MFCs replace the extruded piezoceramic fibres by machined (diced) rectangular fibres of a piezoceramic material. This innovation led to a cheaper and more reliable manufacturing process and allowed direct contact between fibres and electrodes, solving the main problem of permittivity mismatch of PFCs. The original MFC idea developed at NASA [2] used interdigitated electrodes (IDE) to induce the longitudinal or 33 mode in the fibres. But, nowadays, it is possible to find MFCs using uniform field (continuous) electrodes that operate with the transverse or 31 mode in the fibres.

More recently, an alternative MFC design, in which the macro-fibres are oriented perpendicular to the direction of motion, was proposed [4] to induce the transverse shear mode (15 or 35) in the piezoceramic fibres. The transverse shear mode, or thickness shear mode, of piezoceramic materials can be obtained by the application of an electric field that is perpendicular to the remanent polarization direction. This leads to a rotation of the electrical dipoles which induces shear stresses/strains in the material. The transverse shear mode in commercially available piezoceramic patches is normally obtained by polarization along the length or width direction

followed by removal of the electrodes used for polarization and deposition of new electrodes on the top and bottom surfaces. The presence of the new electrodes imposes a dominant electric field, either applied or induced, in the thickness direction, thus perpendicular to the length or width poling direction. Since the mid-1990s, the shear mode of monolithic piezoceramic materials has been considered for applications in the design of smart structures [5–8], including active [9–11] and passive [12, 13] vibration control. From these studies, the shear mode seems to be an interesting alternative for stiffer structures, higher frequencies and non-standard shape deflection patterns.

The main difficulty in the study of MFCs, as an alternative to monolithic piezoceramic patches, is that their behaviour may be much more complex since they are made of several different materials (piezoceramic fibres, epoxy matrix, electrode layers and protective layers). Therefore, it is necessary to understand and model their behaviour to be able to quantify or characterize their effective material properties and, thus, their effectiveness as distributed sensors and actuators. Recently, some research effort has been directed to the identification and characterization of such transducers, in extension (33 or 31) [14–16] and transverse shear (15) [17] modes. It has been shown that the effective properties depend not only on the piezoceramic material used for the fibres and epoxy material used for the matrix and epoxy-to-piezoceramic volume fraction but also on the geometrical and material properties of the other layers (Kapton, acrylic, electrodes). Some analytical methods from the composite materials literature, such as the asymptotic homogenization method (AHM) [17, 18] and the uniform field method (UFM) [3], can be applied to obtain the effective properties of the composite transducer from the properties of its components. Alternatively, one may use techniques based on finite element modelling of the composite transducer to identify its effective properties [19].

In the present work, a finite element homogenization method for a shear actuated d_{15} MFC made of seven layers (Kapton, acrylic, electrode, piezoceramic fibre and epoxy composite, electrode, acrylic, Kapton) is proposed and used for the characterization of its effective material properties. To validate the methodology, first, it is applied to obtain the effective properties of the MFC active layer only, made of piezoceramic fibre and epoxy, and the obtained results are compared to those found using analytical methods [17]. Then, the methodology is applied to the seven-layer MFC.

2. Macro-fibre composites

MFCs that are commercially available use either the 33 or 31 response modes, meaning that the piezoelectric constant that characterizes their actuation/sensing behaviour is respectively the d_{33} or d_{31}, and therefore they are also known as d_{33} or d_{31} MFCs. Schematic representations of the d_{33} and d_{31} MFCs are shown in figures 1 and 2, respectively. The major differences between the two commercially available MFCs are the electrode design and the poling direction of the fibres. In the d_{31} MFC, the poling direction is perpendicular to the fibres (along their thickness) so that transverse extension of the fibres can be obtained through the d_{31} constant. On the other hand, in the d_{33} MFC, the poling direction follows a complex non-uniform distribution according to the disposition of the interdigitated positive and negative electrodes aiming to yield an equivalent macroscopic poling direction parallel to the fibre length, so that longitudinal extension of the fibres can be obtained through the d_{33} constant. The main problem of the d_{33} MFC is that the equivalent macroscopic longitudinal poling direction, and thus its performance, increases with the distance between interdigitated electrode fingers which leads to the requirement of a high actuation voltage (up to 1200 V) to generate the necessary electric field. The d_{31} MFC, on the other hand, requires much lower actuation voltages since the electric field is uniform and in the direction of the actuator thickness, which can be made quite small, but its piezoelectric constant d_{31} is much smaller than d_{33}.

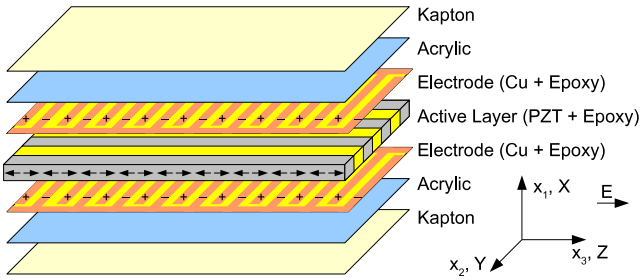

Figure 1. Schematic representation of the longitudinal 'd_{33}' macro-fibre composite.

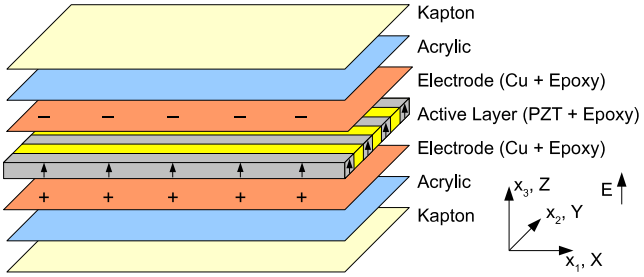

Figure 2. Schematic representation of the transverse 'd_{31}' macro-fibre composite.

The motivations for the development of a d_{15} MFC are to take advantage of the high piezoelectric coupling constant d_{15} that most piezoceramic materials have and the fact that it couples directly to transverse shear strains. The first concept of a d_{15} MFC was recently presented by Raja and Ikeda [4], named as shear actuated fibre composite (SAFC) by the authors, taking advantage of the known fabrication procedures of the d_{31} and d_{33} MFCs. It basically consists of piezoceramic fibres with poling direction perpendicular to the fibre longitudinal axis, as for the d_{33} MFC, but instead of orienting the fibres along the longitudinal direction of the actuator, as for the d_{33} MFC, the fibres are oriented along the width of the actuator so that the poling direction is in the longitudinal direction of the actuator, as shown in figure 3. Different from the proposition of [4], a continuous or woven-

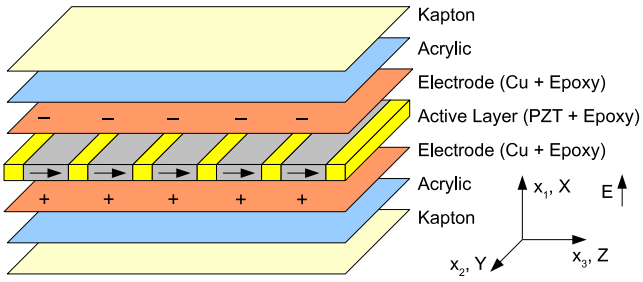

Figure 3. Schematic representation of the thickness shear 'd_{15}' macro-fibre composite.

type electrode, such as those used in commercial d_{31} MFCs, can be used to induce a uniform electric field in the direction of the actuator thickness [17, 20]. As the fibres are poled in their width direction, that is the longitudinal direction of the actuator, a shear strain is induced in the fibres' transversal planes. The width-poled piezoceramic fibres can be made by dice cutting either thickness-poled or longitudinal- or width-poled piezoceramic plates. However, in the first case, proposed by [4], the resulting fibres should be rotated 90° around their axes before positioning them in the epoxy–copper electrode layer, so that the poling direction of each fibre coincides with the longitudinal direction of the actuator, which can be difficult in practice. In the second case, several width-poled plates can be aligned in the polymer film frame before dice cutting of the ensemble leading to a probably cheaper process to produce aligned fibres poled in the width direction, which after packaging would be the longitudinal direction of the actuator.

3. Constitutive equations for shear piezoelectric materials

The shear or d_{15} response mode requires that the poling vector P and measured or applied electric field E be perpendicular to each other. From the modelling point of view, this can be achieved in one way, as in figure 3, by positioning the reference axes such that the poling direction, width of fibre or length of actuator, coincides with direction x_3 or Z and the fibre thickness and actuator thickness coincide with direction x_1 or X. The other way to achieve the d_{15} mode would be to orient the fibre thickness in the x_3 direction and the fibre width and poling in the x_1 direction. The latter has the advantage of using the standard axes orientation for the analysis of thin plates but requires a 90° rotation around the x_2 direction of the standard constitutive equations for piezoelectric materials poled in the x_3 direction. Therefore, for the present work, the former method (as in figure 3) was used to provide easier result interpretation as compared to commercial MFCs and standard piezoelectricity notation.

Starting from the electric enthalpy for a linear orthotropic piezoelectric material poled in the x_3 direction, the constitutive equations can be written in a mixed type form, the so-called e-form, as

$$\left\{\begin{array}{c} T_1 \\ T_2 \\ T_3 \\ T_4 \\ T_5 \\ T_6 \\ \hline D_1 \\ D_2 \\ D_3 \end{array}\right\} = \left[\begin{array}{ccc|ccc|ccc} c_{11}^E & c_{12}^E & c_{13}^E & 0 & 0 & 0 & 0 & 0 & -e_{31} \\ c_{12}^E & c_{22}^E & c_{23}^E & 0 & 0 & 0 & 0 & 0 & -e_{32} \\ c_{13}^E & c_{23}^E & c_{33}^E & 0 & 0 & 0 & 0 & 0 & -e_{33} \\ 0 & 0 & 0 & c_{44}^E & 0 & 0 & 0 & -e_{24} & 0 \\ 0 & 0 & 0 & 0 & c_{55}^E & 0 & -e_{15} & 0 & 0 \\ 0 & 0 & 0 & 0 & 0 & c_{66}^E & 0 & 0 & 0 \\ \hline 0 & 0 & 0 & 0 & e_{15} & 0 & \epsilon_{11}^S & 0 & 0 \\ 0 & 0 & 0 & e_{24} & 0 & 0 & 0 & \epsilon_{22}^S & 0 \\ e_{31} & e_{32} & e_{33} & 0 & 0 & 0 & 0 & 0 & \epsilon_{33}^S \end{array}\right] \times \left\{\begin{array}{c} S_1 \\ S_2 \\ S_3 \\ S_4 \\ S_5 \\ S_6 \\ \hline E_1 \\ E_2 \\ E_3 \end{array}\right\}, \tag{1}$$

where T_p and S_q, with $p, q = 1, \ldots, 6$, denote the six components of mechanical stress and strain in Voigt notation. D_i and E_k, with $i, k = 1, 2, 3$, denote the three components of electric displacement and field. c_{pq}^E, e_{kp} and ϵ_{ik}^S denote the elastic stiffness (at constant electric field), piezoelectric and electric permittivity (at constant mechanical strain) constants.

These constitutive equations can be reduced by considering that the electrodes fully cover the top (x_1^+) and bottom (x_1^-) surfaces so that a preferential or dominant x_1 direction is imposed for the electric field and displacement, such that $E_2 = E_3 = 0$ or $D_2 = D_3 = 0$ (see figure 3). Under this assumption, the reduced constitutive equations can be written in terms of the relevant variables only as

$$\left\{\begin{array}{c} T_1 \\ T_2 \\ T_3 \\ T_4 \\ T_5 \\ T_6 \\ \hline D_1 \end{array}\right\} = \left[\begin{array}{cccccc|c} c_{11}^E & c_{12}^E & c_{13}^E & 0 & 0 & 0 & 0 \\ c_{12}^E & c_{22}^E & c_{23}^E & 0 & 0 & 0 & 0 \\ c_{13}^E & c_{23}^E & c_{33}^E & 0 & 0 & 0 & 0 \\ 0 & 0 & 0 & c_{44}^E & 0 & 0 & 0 \\ 0 & 0 & 0 & 0 & c_{55}^E & 0 & -e_{15} \\ 0 & 0 & 0 & 0 & 0 & c_{66}^E & 0 \\ \hline 0 & 0 & 0 & 0 & e_{15} & 0 & \epsilon_{11}^S \end{array}\right] \times \left\{\begin{array}{c} S_1 \\ S_2 \\ S_3 \\ S_4 \\ S_5 \\ S_6 \\ \hline E_1 \end{array}\right\}. \tag{2}$$

Table 1. Shear mode d_{15} properties of some commercially available piezoceramic materials.

	c_{55}^E (GPa)	$\epsilon_{11}^T/\epsilon_0$	d_{15} (pC N^{-1})	e_{15} (C m^{-2})	k_{15}^2 (%)	k_{15} (%)
APC-840	26.9	1427	480	13.6	49.0	70
APC-850	21.8	1851	590	13.2	46.2	68
APC-855	22.4	3012	720	15.0	43.6	66
EC-76	21.9	2853	730	16.0	46.2	68
EC-64	25.7	1436	506	13.0	51.8	72
PIC-255	21.0	1650	550	11.6	43.6	66
PZT-5H	23.0	3130	740	17.0	45.6	68
PZT-5A	21.1	1730	584	12.3	46.9	68
PZT-7A	29.4	930	360	10.6	46.2	68
Sonox-P502	30.1	1950	560	16.9	54.8	74
Sonox-P504	24.8	1920	530	13.2	43.6	66
Sonox-P508	29.8	1700	550	16.4	50.4	71

Hence, the electromechanical coupling is between the electric field and the displacement in the x_1 direction and the x_1–x_3 shear stress and strain. The electromechanical coupling coefficient can be defined from the value of the coupling or interaction coefficient relative to the principal or diagonal coefficients [21] using the standard intensive type or d-form of the constitutive equations, such that

$$k_{15}^2 = \frac{d_{15}^2}{s_{55}^E \epsilon_{11}^T}, \tag{3}$$

where

$$d_{15} = e_{15}/c_{55}^E, \quad s_{55}^E = 1/c_{55}^E, \quad \text{and} \quad \epsilon_{11}^T = \epsilon_{11}^S + e_{15}^2/c_{55}^E. \tag{4}$$

This expression can be also written in terms of the e_{15} constant present in the e-form of the constitutive equations but, since this is a mixed type of the constitutive equations, one of the principal constants should be taken from another form of the constitutive equations in order to obtain a formula similar to (3). A modification of (3) can, however, be considered in terms of the principal constants only:

$$k_{15}^2 = \frac{e_{15}^2}{c_{55}^E \epsilon_{11}^T} = \frac{e_{15}^2}{c_{55}^D \epsilon_{11}^S} = \frac{e_{15}^2}{c_{55}^E \epsilon_{11}^S + e_{15}^2}. \tag{5}$$

This expression and its variations can also be found by using the relations between the constants appearing in different forms of the constitutive equations such as

$$k_{15}^2 = 1 - c_{55}^E/c_{55}^D = 1 - \epsilon_{11}^S/\epsilon_{11}^T. \tag{6}$$

It is thus clear that the material properties d_{15}, c_{55}^E and ϵ_{11}^T are of major importance for the evaluation of the potential of such material as a candidate for the development of transducers (actuators and sensors). Table 1 presents typical values of these constants for a number of commercially available piezoceramic materials, calculated using the respective material data sheets from the manufacturers [22–26].

In the case of the d_{15} MFC which is composed of a number of different materials, it is important to identify the effective properties of the ensemble based on the properties of its constituents. For that, the representative volume element (RVE) technique together with Ansys® finite element software is used first for the active layer alone and then for the multilayer transducer. The effective properties obtained are compared to those from previous works using analytical homogenization techniques [17].

4. Active layer effective material properties

4.1. Analytical homogenization using UFM and AHM

The asymptotic homogenization method (AHM) can be used to model the d_{15} MFC active layer considering that it is made of identical unit cells periodically distributed along the poling direction. Asymptotical expansions of mechanical displacements and electric potential are used to provide asymptotical expansions of mechanical stresses and electric displacements and to solve the equilibrium equations of the heterogeneous active layer. Then, comparison of the resulting equations with the averaged ones leads to the solution of periodic functions of the local variable from which the effective constants, or effective constitutive equations, can be written [17, 18].

The uniform field method (UFM) is based on the assumption that selected different fields are uniform in the constituents of the heterogeneous media. It is a generalization of the well known rules of mixtures which use parallel and series additions to model effective properties of two-phase materials [3]. The resulting effective coefficients are thus dependent on the assumptions considered for selecting the field variables that are uniform (equal) in the two phases and, thus, also equal to the average field variables. Then, the corresponding dual field variables are evaluated through linear combination of the field variables of each phase in terms of the fibre volume fraction (FVF). Rearranging the natural and conjugate variables as desired, the corresponding constitutive equations can be written in terms of the constituents' material constants and the fibre volume fraction.

4.2. Finite element numerical homogenization

In this section, a numerical homogenization using the finite element method is applied to the d_{15} MFC active layer RVE [19, 27]. It consists in imposing relative mechanical displacement and electric potential boundary conditions on the boundaries of the RVE (X_1^-, X_1^+, X_2^-, X_2^+, X_3^-, X_3^+). In the case of the RVE considered for the d_{15} MFC active layer, shown in figure 4, these boundaries are X_1^-: $x_1 = 0$, X_1^+: $x_1 = h_P$, X_2^-: $x_2 = 0$, X_2^+: $x_2 = w$, X_3^-: $x_3 = 0$, X_3^+: $x_3 = L_P + L_E$. Continuous electrodes are considered on the surfaces $X_1^{e-} = X_1^-$ and $X_1^{e+} = X_1^+$.

Average strains and electric fields can therefore be imposed on the RVE using displacements and voltage boundary conditions, such that

$$u_i^{X_j^+} - u_i^{X_j^-} = \bar{S}_{ij}(x_j^{X_j^+} - x_j^{X_j^-}), \qquad i, j = 1, 2, 3, \tag{7}$$

and

$$\phi^{X_n^+} - \phi^{X_n^-} = -\bar{E}_n(x_n^{X_n^+} - x_n^{X_n^-}), \qquad n = 1, 2, 3. \tag{8}$$

Table 2. Boundary conditions (displacement/electric potential) and relations used to evaluate the effective material properties of a d_{15} piezoelectric MFC.

Problem	X_1^-/X_1^+	X_2^-/X_2^+	X_3^-/X_3^+	X_1^{e-}/X_1^{e+}	Relation
1	$u_1^{i+} - u_1^{i-} = q$	$u_2^{i+} - u_2^{i-} = 0$	$u_3^{i+} - u_3^{i-} = 0$	—	$c_{1j}^E = \bar{T}_j/\bar{S}_1$ (13)
	—	$\phi^{i+} - \phi^{i-} = 0$	$\phi^{i+} - \phi^{i-} = 0$	$\phi^{i+} = 0;\ \phi^{i-} = 0$	
2	$u_1^{i+} - u_1^{i-} = 0$	$u_2^{i+} - u_2^{i-} = q$	$u_3^{i+} - u_3^{i-} = 0$	—	$c_{2j}^E = \bar{T}_j/\bar{S}_2$ (13)
	—	$\phi^{i+} - \phi^{i-} = 0$	$\phi^{i+} - \phi^{i-} = 0$	$\phi^{i+} = 0;\ \phi^{i-} = 0$	
3	$u_1^{i+} - u_1^{i-} = 0$	$u_2^{i+} - u_2^{i-} = 0$	$u_3^{i+} - u_3^{i-} = q$	—	$c_{3j}^E = \bar{T}_j/\bar{S}_3$ (13)
	—	$\phi^{i+} - \phi^{i-} = 0$	$\phi^{i+} - \phi^{i-} = 0$	$\phi^{i+} = 0;\ \phi^{i-} = 0$	
4	$u_1^{i+} - u_1^{i-} = 0$	$u_3^{i+} - u_3^{i-} = q$	$u_2^{i+} - u_2^{i-} = q$	—	$c_{44}^E = \bar{T}_4/\bar{S}_4$ (14)
	—	$\phi^{i+} - \phi^{i-} = 0$	$\phi^{i+} - \phi^{i-} = 0$	$\phi^{i+} = 0;\ \phi^{i-} = 0$	
5	$u_3^{i+} - u_3^{i-} = q$	$u_2^{i+} - u_2^{i-} = 0$	$u_1^{i+} - u_1^{i-} = q$	—	$c_{55}^E = \bar{T}_5/\bar{S}_5$ (14)
	—	$\phi^{i+} - \phi^{i-} = 0$	$\phi^{i+} - \phi^{i-} = 0$	$\phi^{i+} = 0;\ \phi^{i-} = 0$	$e_{15} = \bar{D}_1/\bar{S}_5$ (15)
6	$u_2^{i+} - u_2^{i-} = q$	$u_1^{i+} - u_1^{i-} = q$	$u_3^{i+} - u_3^{i-} = 0$	—	$c_{66}^E = \bar{T}_6/\bar{S}_6$ (14)
	—	$\phi^{i+} - \phi^{i-} = 0$	$\phi^{i+} - \phi^{i-} = 0$	$\phi^{i+} = 0;\ \phi^{i-} = 0$	
7	—	—	—	—	$d_{15} = \bar{S}_5/\bar{E}_1$ (16)
	—	$\phi^{i+} - \phi^{i-} = 0$	$\phi^{i+} - \phi^{i-} = 0$	$\phi^{i+} = 0;\ \phi^{i-} = q$	$\epsilon_{11}^T = \bar{D}_1/\bar{E}_1$ (16)

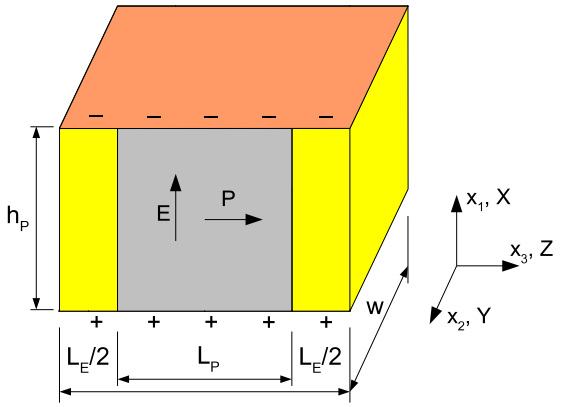

Figure 4. Representative volume element (RVE) for the active layer of the d_{15} MFC.

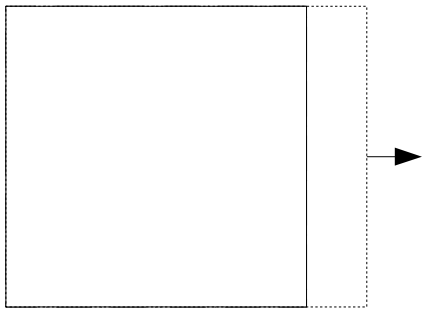

Figure 5. Plane representation of the local problem used to evaluate the elastic constants related to normal strains and stresses.

The resulting average strains, stresses, electric fields and electric displacements in the RVE are defined as

$$\bar{S}_q = \frac{1}{V}\int_V S_q \,\mathrm{d}V, \qquad \text{and} \qquad \bar{T}_p = \frac{1}{V}\int_V T_p \,\mathrm{d}V, \quad \text{with } p, q = 1, \ldots, 6, \tag{9}$$

$$\bar{E}_k = \frac{1}{V}\int_V E_k \,\mathrm{d}V, \qquad \text{and} \qquad \bar{D}_i = \frac{1}{V}\int_V D_i \mathrm{d}V, \quad \text{with } i, k = 1, 2, 3. \tag{10}$$

These integrals are approximated in Ansys® by a sum over averaged element values multiplied by the respective element volume divided by the total volume of the RVE, such that

$$\bar{S}_q = \frac{\sum_{e=1}^N S_q^{(e)} V^{(e)}}{\sum_{e=1}^N V^{(e)}}, \qquad \text{and} \qquad \bar{T}_p = \frac{\sum_{e=1}^N T_p^{(e)} V^{(e)}}{\sum_{e=1}^N V^{(e)}}, \quad \text{with } p, q = 1, \ldots, 6, \tag{11}$$

$$\bar{E}_k = \frac{\sum_{e=1}^N E_k^{(e)} V^{(e)}}{\sum_{e=1}^N V^{(e)}}, \qquad \text{and} \qquad \bar{D}_i = \frac{\sum_{e=1}^N D_i^{(e)} V^{(e)}}{\sum_{e=1}^N V^{(e)}}, \quad \text{with } i, k = 1, 2, 3, \tag{12}$$

where $V^{(e)}$ is the volume of the element e. $S_q^{(e)}$, $T_p^{(e)}$, $E_k^{(e)}$ and $D_i^{(e)}$ are the average strains, stresses, electric fields and electric displacements evaluated at element e. N is the total number of finite elements used to discretize the RVE.

For the evaluation of the elastic constants related to normal strains and stresses c_{pq}^E, $p, q = 1, 2, 3$, three local problems are analysed for which a normal strain S_q ($q = 1, 2, 3$) is applied by imposing relative normal displacements $u_q^{X_q^+} - u_q^{X_q^-}$ (figure 5). In order to obtain $\bar{S}_j = 0$ if $j \neq q$, the normal displacements u_j for each pair of nodes at opposing surfaces X_j^- and X_j^+ are set to be equal (symmetrically coupled degrees of freedom). To ensure a short circuit electric boundary condition, the voltage degrees of freedom in the electrodes at surfaces X_1^- and X_1^+ are set to zero. Table 2 indicates symmetric boundary conditions for the electric potential along directions x_2 and x_3 for the corresponding X_2^-/X_2^+ and X_3^-/X_3^+ RVE surfaces. Then, considering the constitutive equations in (2), the effective elastic constants are evaluated using the following expression:

$$c_{pq}^E = \bar{T}_p/\bar{S}_q, \qquad p, q, = 1, 2, 3, \tag{13}$$

where the average stresses $\bar{T}_p$ and strains $\bar{S}_q$ are evaluated using (11).

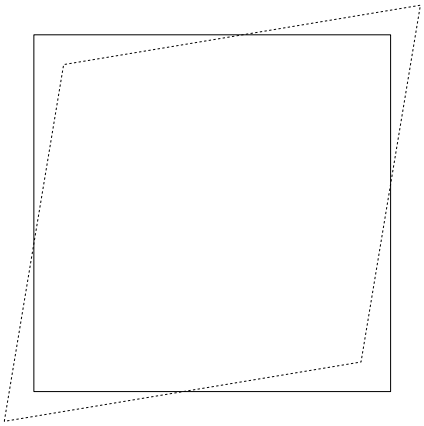

Figure 6. Plane representation of the local problem used to evaluate the elastic constants related to shear strains and stresses.

For the evaluation of the elastic constants related to shear strains and stresses c^E_{pp}, $p = 4, 5, 6$, another three local problems are analysed for which shear strains S_{ik} ($S_{23} = S_4/2$, $S_{13} = S_5/2$ and $S_{12} = S_6/2$) are applied to approximate a pure shear stress state in the planes $x_2 - x_3$, $x_1 - x_3$ and $x_1 - x_2$ by imposing relative shear displacements $u_i^{X_k^+} - u_i^{X_k^-}$ at surfaces X_k^+/X_k^- and $u_k^{X_i^+} - u_k^{X_i^-}$ at surfaces X_i^+/X_i^- (figure 6). Moreover, the normal displacements at the boundary surfaces parallel to each shear plane of interest are symmetrically coupled to ensure zero strains perpendicular to the shear plane. To ensure a short circuit electric boundary condition, the voltage degrees of freedom in the electrodes at surfaces X_1^- and X_1^+ are set to zero. Table 2 indicates symmetric boundary conditions for the electric potential along directions x_2 and x_3 for the corresponding X_2^-/X_2^+ and X_3^-/X_3^+ RVE surfaces. Therefore, the effective elastic constants are evaluated in terms of the average shear stresses $\bar{T}_p$ and strains $\bar{S}_p$ using

$$c^E_{pp} = \bar{T}_p/\bar{S}_p, \qquad p = 4, 5, 6. \tag{14}$$

The piezoelectric constant e_{15} can be also obtained from the local problem used to evaluate c^E_{55}, that is where a pure shear stress state in the plane x_1–x_3 is approximated. From the constitutive equations (2), e_{15} can be obtained by evaluating the average electric displacement D_1 such that

$$e_{15} = \bar{D}_1/\bar{S}_5, \tag{15}$$

where the average shear strain $\bar{S}_5$ and electric displacement $\bar{D}_1$ are evaluated using the approximation of (11) and (12).

For the evaluation of the piezoelectric and dielectric constants of the d-form, d_{15} and ϵ^T_{11}, another local problem is set up for which an electric voltage $\phi^{X_1^+} = h_P$ (in value) is applied to the electrode at surface X_1^+ while the voltage at the opposite surface (X_1^-) is set to zero so that a unitary electric field in the x_1 direction is generated (figure 7). To approximate the condition of zero stresses in the RVE, no restriction is made to the displacements in the RVE except for the origin where all displacements are set to zero to prevent rigid body displacements. Then, considering zero shear stress

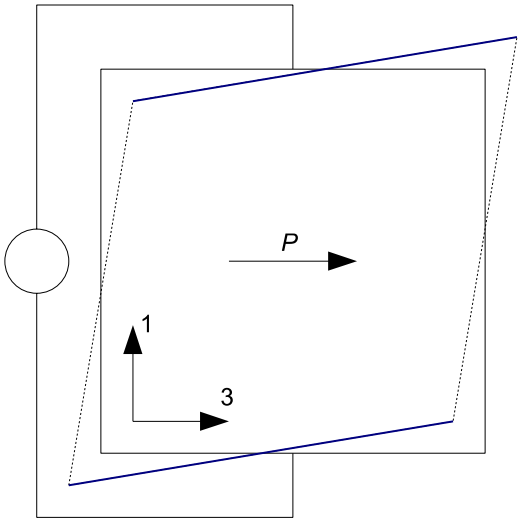

Figure 7. Plane representation of the local problem used to evaluate the piezoelectric and dielectric constants related to the shear response mode.

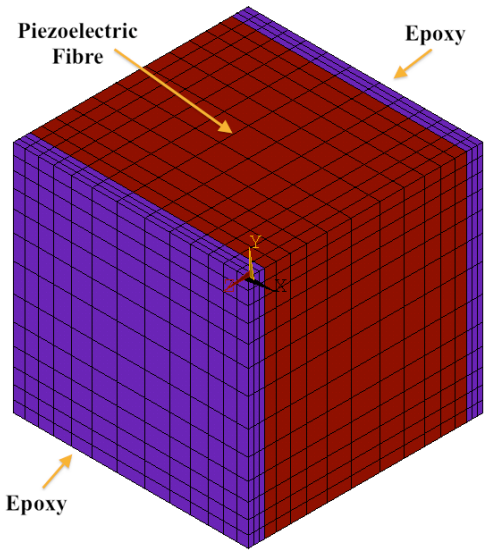

Figure 8. Finite element mesh for the d_{15} MFC active layer RVE.

T_5 in the d-form of the constitutive equations, the piezoelectric and dielectric constants, d_{15} and ϵ^T_{11}, can be evaluated from

$$d_{15} = \bar{S}_5/\bar{E}_1, \tag{16}$$

and

$$\epsilon^T_{11} = \bar{D}_1/\bar{E}_1. \tag{17}$$

Table 2 summarizes the local problems used for the characterization of the relevant material properties of the d_{15} MFC active layer RVE. u_j^{i-} and u_j^{i+} are the displacements in direction j and ϕ^{i-} and ϕ^{i+} are the electric potentials at the ith node of the opposite surfaces. q is an arbitrary non-null value.

Other effective piezoelectric and dielectric material constants, such as e_{31}, e_{32}, e_{33}, e_{24}, ϵ^T_{22} and ϵ^T_{33}, are normally evaluated in the literature. This could be done by changing the position of the electrodes, leading to other simplifying

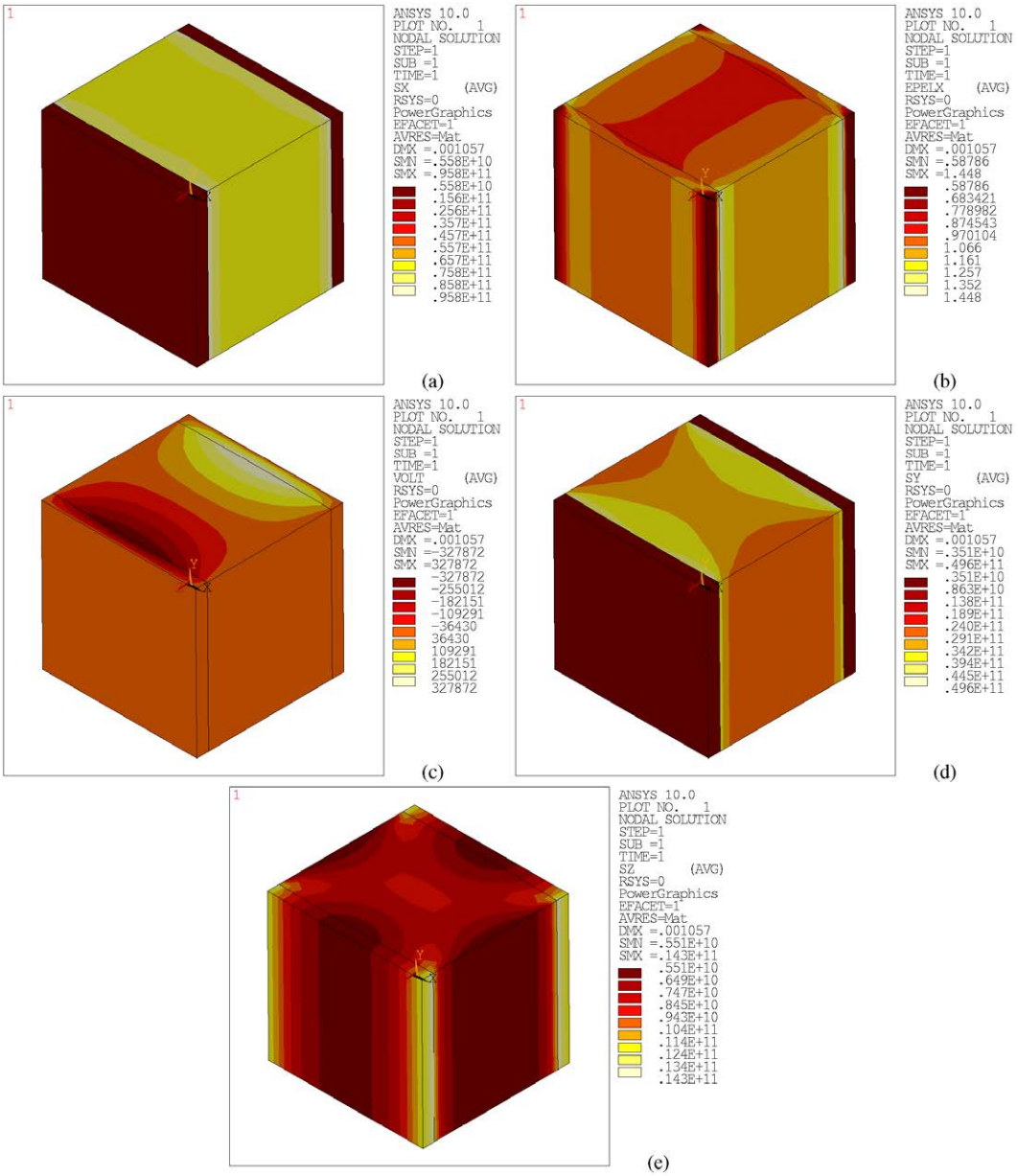

Figure 9. Distributions induced by a unitary normal strain $S_1 = (u_1^{X_1^+} - u_1^{X_1^-})/h_P = 1$ (problem 1) applied to the d_{15} MFC active layer RVE: (a) normal stress T_1, (b) normal strain S_1, (c) electric potential, (d) normal stress T_2 and (e) normal stress T_3.

assumptions for the electric boundary conditions (either $E_k = 0$ or $D_k = 0$ for $k \neq 2$ or $k \neq 3$, instead of $E_k = 0$ or $D_k = 0$ for $k \neq 1$ as in this work). However, this was not done in this work since it is focused on the proposed shear d_{15} MFC design which is only operational with electrodes over surfaces X_1^- and X_1^+. Therefore, it is impossible to apply or measure electric field or electric displacement in directions 2 and 3.

Figure 8 shows the finite element mesh used in Ansys® for the d_{15} MFC active layer RVE using an FVF of 0.86. The 3D 20-node coupled-field solid finite element SOLID226 was used to mesh all volumes. This element has four degrees of freedom per node, the three Cartesian nodal displacements and the nodal electric potential. 2873 finite elements were used considering 13 divisions in the x_1 and x_2 directions and 17 divisions in the x_3 direction (11 divisions for the PZT layer and three divisions for each epoxy layer). According to figure 4, the dimensions considered for this RVE are $h_P = 1$ mm, $L_P = 0.860$ mm, $L_E = 0.140$ mm, $w = 1$ mm. The material properties for the piezoceramic material Sonox-P502, taken from [14], are $s_{11}^E = s_{22}^E = 18.5$ p m^2 N^{-1}, $s_{33}^E = 20.7$ p m^2 N^{-1}, $s_{12}^E = -6.29$ p m^2 N^{-1}, $s_{13}^E = -6.23$ p m^2 N^{-1}, $s_{44}^E = s_{55}^E = 33.2$ p m^2 N^{-1}, $s_{66}^E = 52.3$ p m^2 N^{-1}, $d_{31} = d_{32} = -185$ pC N^{-1}, $d_{33} = 440$ pC N^{-1}, $d_{15} = d_{24} = 560$ pC N^{-1}, $\epsilon_{11}^T = \epsilon_{22}^T = 1950\epsilon_0$, $\epsilon_{33}^T = 1850\epsilon_0$. The material properties for the isotropic epoxy are $Y = 2.9$ GPa, $\nu = 0.3$ and $\epsilon = 4.25\epsilon_0$.

The distributions of normal and shear stresses and strains for the local problems used to evaluate the effective elastic properties of the RVE using an FVF of 0.86 are presented in figures 9–14. As expected, in the first two local problems

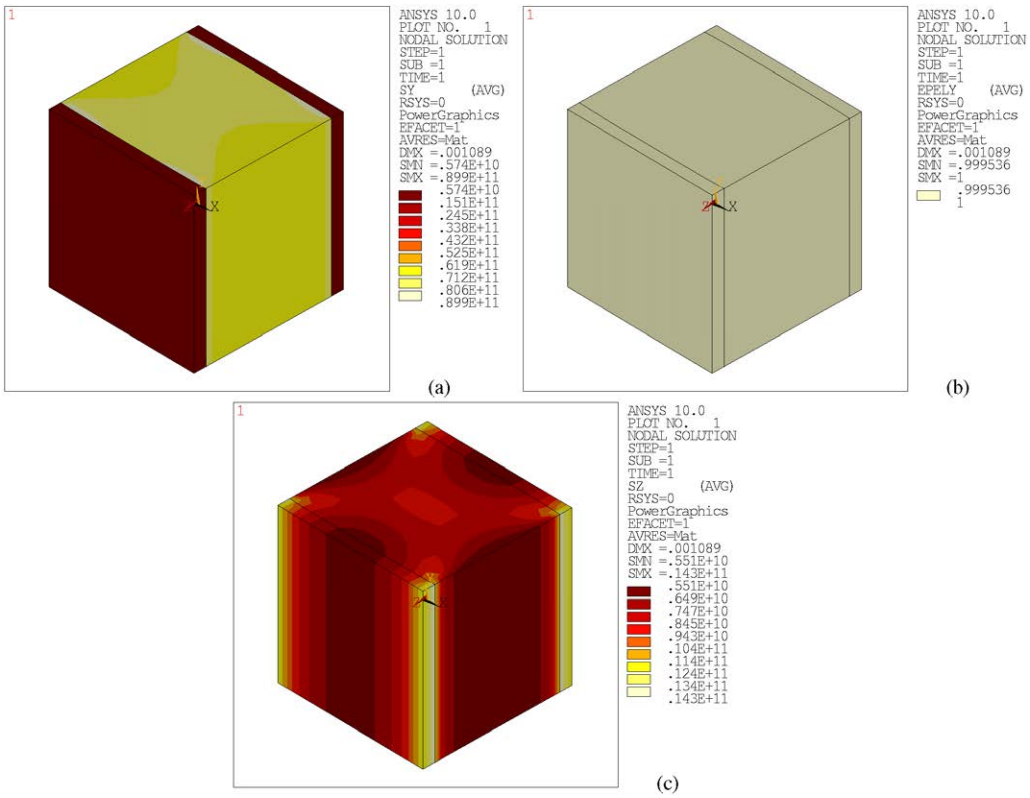

Figure 10. Distributions induced by a unitary normal strain $S_2 = (u_2^{X_2^+} - u_2^{X_2^-})/w = 1$ (problem 2) applied to the d_{15} MFC active layer RVE: (a) normal stress T_2, (b) normal strain S_2 and (c) normal stress T_3.

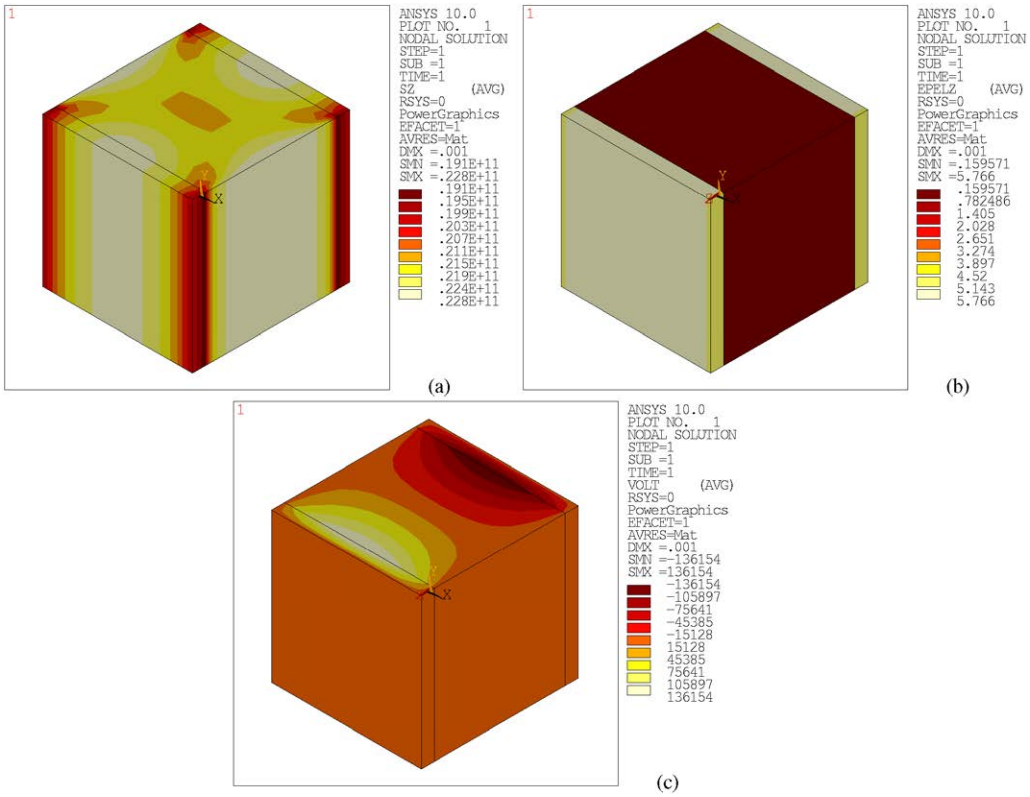

Figure 11. Distributions induced by a unitary normal strain $S_3 = (u_3^{X_3^+} - u_3^{X_3^-})/(L_P + L_E) = 1$ (problem 3) applied to the d_{15} MFC active layer RVE: (a) normal stress T_3, (b) normal strain S_3 and (c) electric potential.

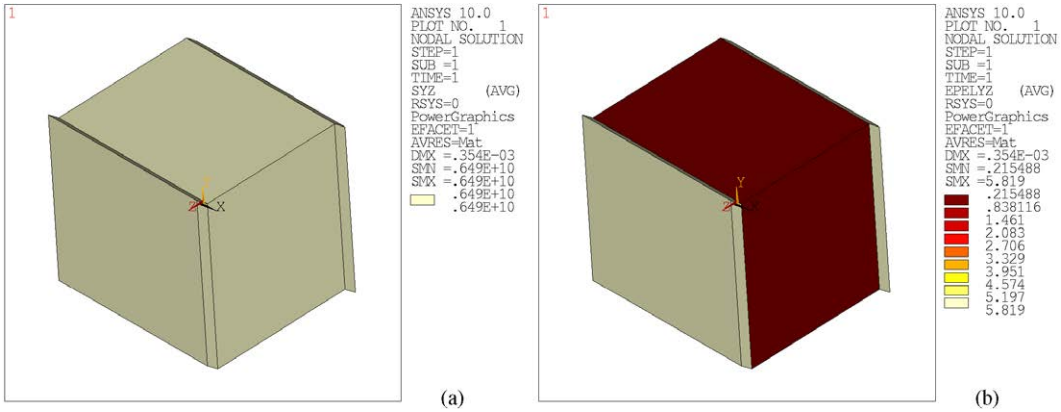

Figure 12. Distributions induced by a unitary shear strain $S_4 = 1$ (problem 4) applied to the d_{15} MFC active layer RVE: (a) shear stress T_4 and (b) shear strain S_4.

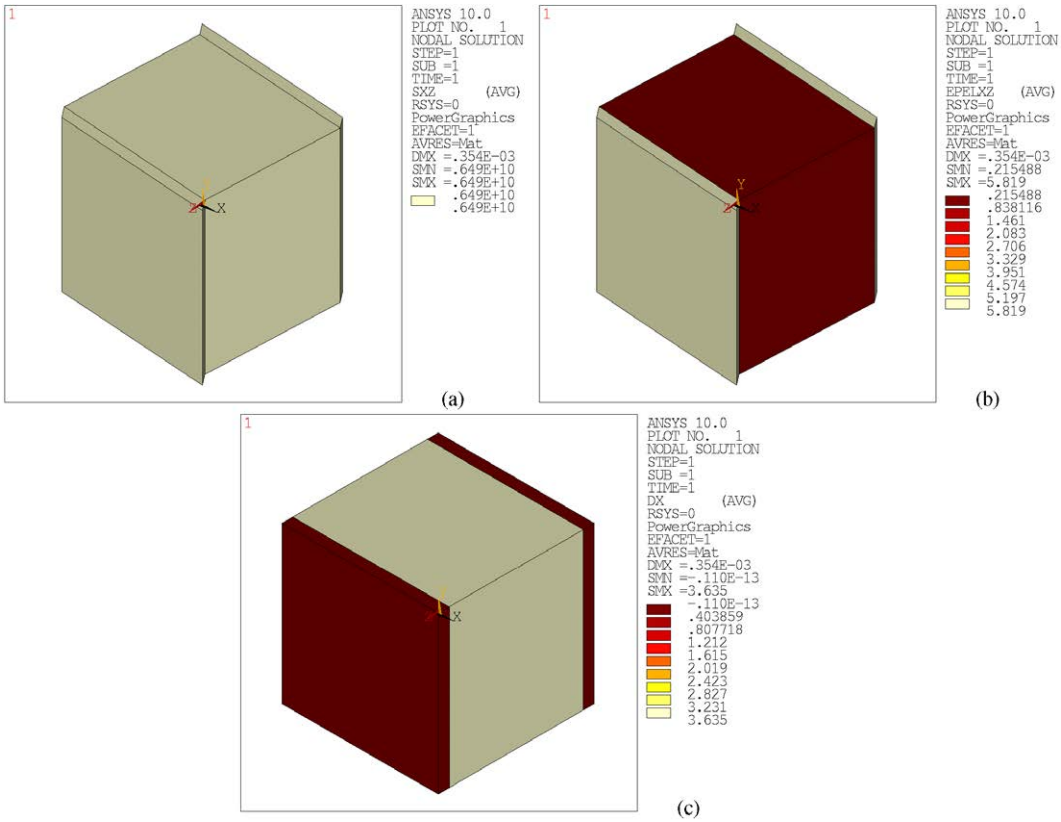

Figure 13. Distributions induced by a unitary shear strain $S_5 = 1$ (problem 5) applied to the d_{15} MFC active layer RVE: (a) shear stress T_5, (b) shear strain S_5 and (c) electric displacement D_1.

(T_1, figure 9(a), and T_2, figure 10(a)), the stress is concentrated in the piezoceramic fibre. On the other hand, in the third local problem (T_3, figure 11(a)), the stress is relatively well distributed in the RVE while the strain is much higher in the epoxy material (i.e. almost all deformation is due to the softer epoxy material, figure 11(b)). The deformation is also dominated by the epoxy material in the local problems related to shear elastic constants in planes yz, c^E_{44} (figure 12(b)), and xz, c^E_{55} (figure 13(b)). On the other hand, in the local problem for the evaluation of c^E_{66} (figure 14), the strain is homogeneous while the stress is concentrated in the piezoceramic fibre.

From figure 9(b), one may also notice that the normal strain S_1 is not homogeneous. This may be due to the non-homogeneous electric potential induced in the piezoceramic by the grounded electrodes in X_1^- and X_1^+ (figure 9(c)). This can be explained by the fact that the piezoceramic fibre is stiffened where an electric potential is induced and, thus, the effective stiffness of the piezoceramic fibre near the electrodes is smaller. The same effect leads to a non-homogeneous distribution of the normal stress T_3 (figure 11(a)), although the non-homogeneity is less pronounced than for S_1 strains. For the second local problem (T_2/S_2, figure 10), the effect of the

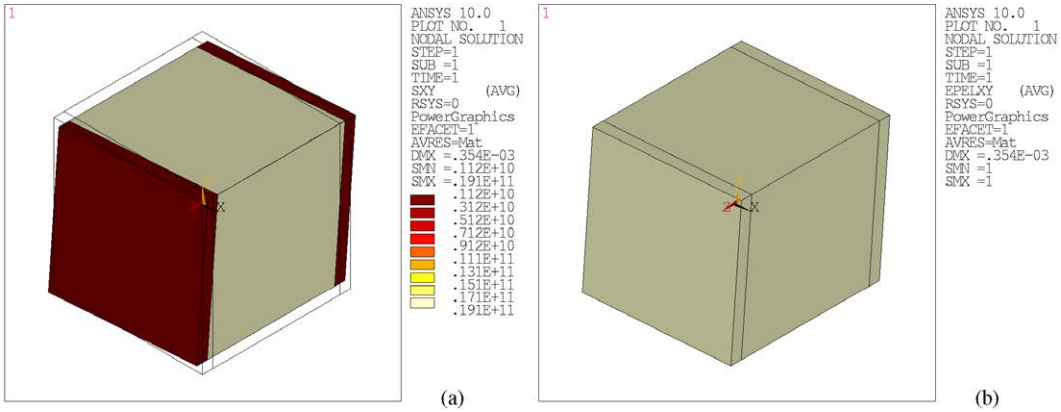

Figure 14. Distributions induced by a unitary shear strain $S_6 = 1$ (problem 6) applied to the d_{15} MFC active layer RVE: (a) shear stress T_6 and (b) shear strain S_6.

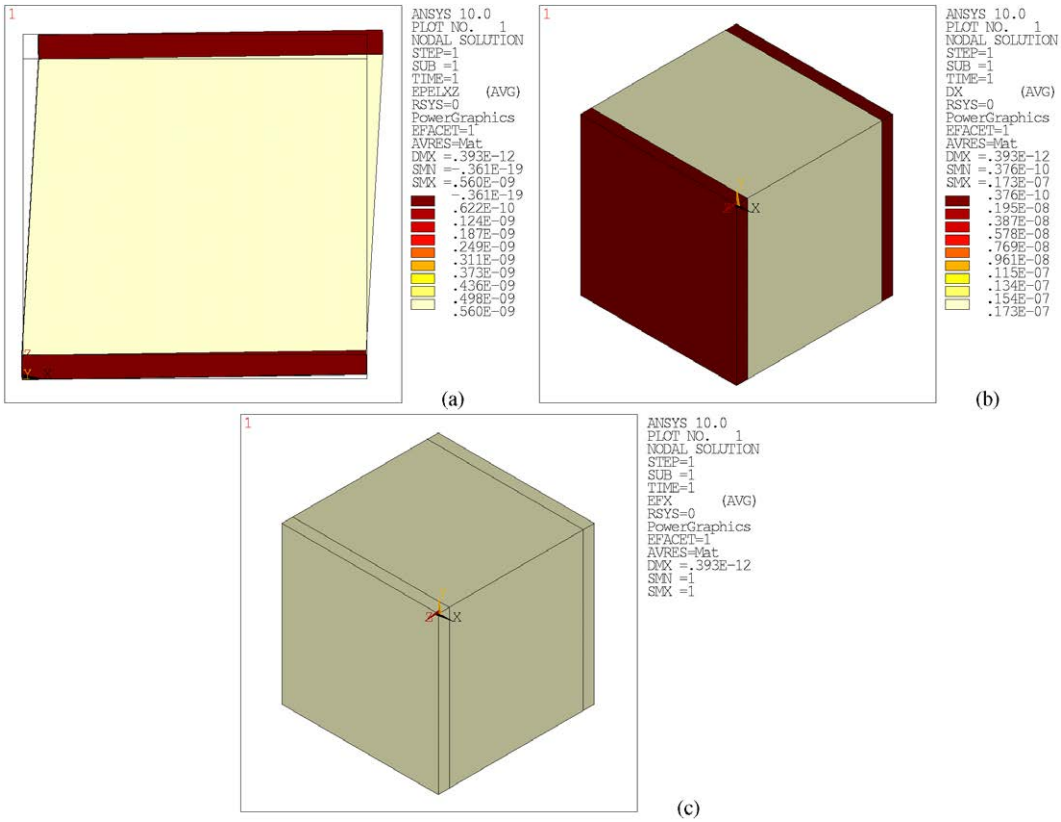

Figure 15. Distributions induced by a unitary electric field $E_1 = (\phi^{X_1^+} - \phi^{X_1^-})/h_P = 1$ applied to the d_{15} MFC active layer RVE: (a) shear strain S_5, (b) electric displacement D_1 and (c) electric field E_1.

non-homogeneous induced potential is negligible. For the last three local problems (T_4/S_4, figure 12; T_5/S_5, figure 13; and T_6/S_6, figure 14), the induced potential itself was found to be negligible.

The distribution of shear strain S_5 and electric displacement D_1 for the local problem used to evaluate the effective piezoelectric and dielectric properties, d_{15} and ϵ_{11}^T, of the RVE using an FVF of 0.86 are presented in figure 15. Their distributions are as expected from the UFM. It is noticeable that only the piezoceramic fibre is deformed, to a pure shear strain state, by the applied difference of electric potential. Moreover, as expected, the electric displacement is also concentrated in the piezoceramic fibre (figure 15(b)). A unitary electric field, however, is equally distributed over the RVE since it is considered that the electrodes cover the entire surfaces X_1^- and X_1^+, that is both the piezoceramic fibre and the epoxy material (figure 15(c)).

Table 3 shows the effective properties, transformed to Voigt notation, of the d_{15} MFC active layer using an FVF of 0.86 obtained by the finite element local problems. The table also shows the corresponding results obtained by the analytical homogenization methods UFM (without the

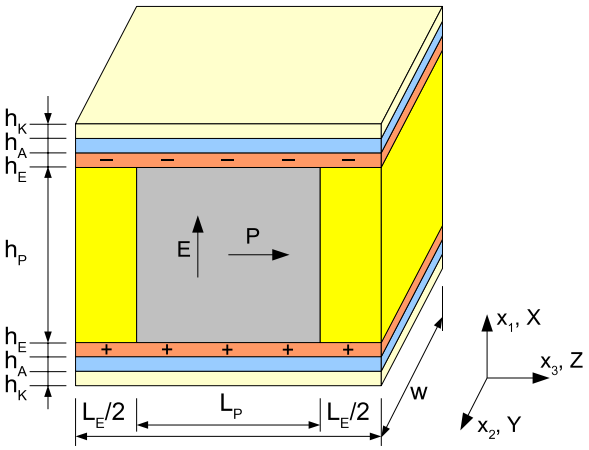

Figure 16. Representative volume element (RVE) for a d_{15} MFC.

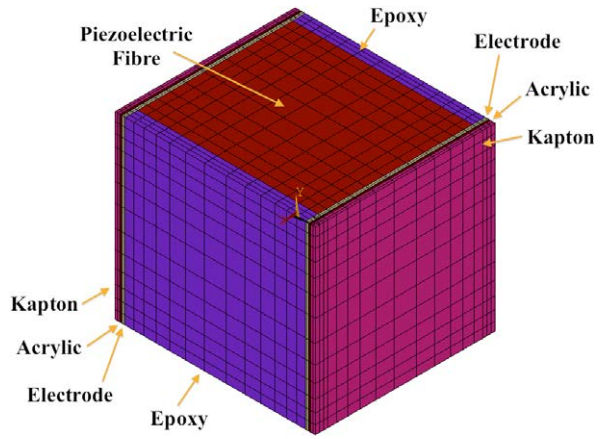

Figure 17. Finite element mesh for the seven-layered d_{15} MFC RVE.

Table 3. Effective short circuit elastic and piezoelectric properties of the d_{15} MFC active layer (FVF = 0.86).

Ansys® FE	UFM [17]	AHM (UDEF) [17]
$Y_1 = 50.09$ GPa	$Y_1 = 52.76$ GPa	$Y_1 = 46.90$ GPa
$Y_2 = 50.09$ GPa	$Y_2 = 52.76$ GPa	$Y_2 = 46.90$ GPa
$Y_3 = 20.52$ GPa	$Y_3 = 22.49$ GPa	$Y_3 = 17.98$ GPa
$G_{23} = 6.49$ GPa	$G_{23} = 5.89$ GPa	$G_{23} = 5.89$ GPa
$G_{13} = 6.49$ GPa	$G_{13} = 5.89$ GPa	$G_{13} = 5.89$ GPa
$G_{12} = 16.60$ GPa	$G_{12} = 16.61$ GPa	$G_{12} = 16.61$ GPa
$\nu_{12} = 0.43$	$\nu_{12} = 0.59$	$\nu_{12} = 0.41$
$\nu_{13} = 0.20$	$\nu_{13} = 0.19$	$\nu_{13} = 0.41$
$\nu_{23} = 0.20$	$\nu_{23} = 0.19$	$\nu_{23} = 0.41$
$d_{15} = 481.60$ pC N^{-1}	$d_{15} = 481.60$ pC N^{-1}	$d_{15} = 481.60$ pC N^{-1}
$e_{15} = 3.13$ C m^{-2}	$e_{15} = 2.84$ C m^{-2}	$e_{15} = 2.84$ C m^{-2}
$\epsilon_{11}^T = 14.85$ nF m^{-1}	$\epsilon_{11}^T = 14.85$ nF m^{-1}	$\epsilon_{11}^T = 14.85$ nF m^{-1}
$k_{15}^2 = 10.1\%$	$k_{15}^2 = 9.2\%$	$k_{15}^2 = 9.2\%$
$k_{15} = 32\%$	$k_{15} = 30\%$	$k_{15} = 30\%$

Table 4. Effective short circuit elastic and piezoelectric properties of the d_{15} MFC active layer (FVF = 0.95).

Ansys® FE	UFM [17]	AHM (UDEF) [17]
$Y_1 = 54.81$ GPa	$Y_1 = 57.74$ GPa	$Y_1 = 51.50$ GPa
$Y_2 = 54.81$ GPa	$Y_2 = 57.74$ GPa	$Y_2 = 51.50$ GPa
$Y_3 = 37.40$ GPa	$Y_3 = 45.44$ GPa	$Y_3 = 30.16$ GPa
$G_{23} = 13.09$ GPa	$G_{23} = 10.68$ GPa	$G_{23} = 10.68$ GPa
$G_{13} = 13.09$ GPa	$G_{13} = 10.68$ GPa	$G_{13} = 10.68$ GPa
$G_{12} = 18.22$ GPa	$G_{12} = 18.23$ GPa	$G_{12} = 18.23$ GPa
$\nu_{12} = 0.43$	$\nu_{12} = 0.58$	$\nu_{12} = 0.41$
$\nu_{13} = 0.21$	$\nu_{13} = 0.20$	$\nu_{13} = 0.43$
$\nu_{23} = 0.21$	$\nu_{23} = 0.20$	$\nu_{23} = 0.43$
$d_{15} = 532.00$ pC N^{-1}	$d_{15} = 532.00$ pC N^{-1}	$d_{15} = 532.00$ pC N^{-1}
$e_{15} = 6.97$ C m^{-2}	$e_{15} = 5.68$ C m^{-2}	$e_{15} = 5.68$ C m^{-2}
$\epsilon_{11}^T = 16.40$ nF m^{-1}	$\epsilon_{11}^T = 16.40$ nF m^{-1}	$\epsilon_{11}^T = 16.40$ nF m^{-1}
$k_{15}^2 = 22.6\%$	$k_{15}^2 = 18.4\%$	$k_{15}^2 = 18.4\%$
$k_{15} = 48\%$	$k_{15} = 43\%$	$k_{15} = 43\%$

unidirectional electric field, UDEF, approximation) and AHM (with the UDEF approximation) [17] for comparison. The effective electromechanical coupling coefficient of the RVE k_{15} is evaluated from the effective elastic, piezoelectric and dielectric properties, c_{55}^E, d_{15} and ϵ_{11}^T, using (3). Notice that the numerically evaluated effective properties match quite well with those evaluated using analytical homogenization techniques. In particular, the Young moduli obtained numerically stand between those evaluated with the UFM (without UDEF) and AHM (with UDEF) methods. The shear modulus of major interest for the d_{15} MFC, G_{13}, is 10% higher than the analytical results. For this reason, the squared effective electromechanical coefficient obtained numerically is a little higher than the one obtained analytically (10% compared to 9%). The same reason explains the fact that the numerical e_{15} value is higher than the analytical one.

A similar analysis was performed augmenting the fibre volume fraction of the d_{15} MFC active layer RVE to 0.95 (as recommended in [17]). This was done by modifying the RVE dimensions to $h_P = 1$ mm, $L_P = 0.950$ mm, $L_E = 0.050$ mm, $w = 1$ mm. Table 4 shows the effective properties of the d_{15} MFC active layer using an FVF of 0.95 obtained numerically, using finite element homogenization, and analytically, using the UFM (without UDEF) and AHM (with UDEF) methods [17]. As in the previous case, the numerically evaluated effective properties match quite well with those evaluated using analytical homogenization techniques. These results also show that the increase in the FVF from 0.86 to 0.95, meaning a 10% increase, leads to an overall increase in the elastic (stiffness) constants of the RVE. More importantly, the effective piezoelectric properties of major interest to the d_{15} MFC, d_{15} or e_{15}, increase substantially by 10% and 123%, respectively. This yields an increase in the effective squared electromechanical coupling coefficient k_{15}^2 by 123%, from 10.1% to 22.6%.

5. d_{15} MFC effective material properties

In this section, the finite element homogenization method is applied to evaluate the effective properties of a d_{15} MFC including the electrode and protective layers, according to the schematic representation of figure 3. As in section 4, this is done here by considering an RVE of the d_{15} MFC, as shown in figure 16. The protective layers, made of Kapton and acrylic materials, and the electrode layer, made of copper and epoxy, are considered isotropic. Therefore, the finite element

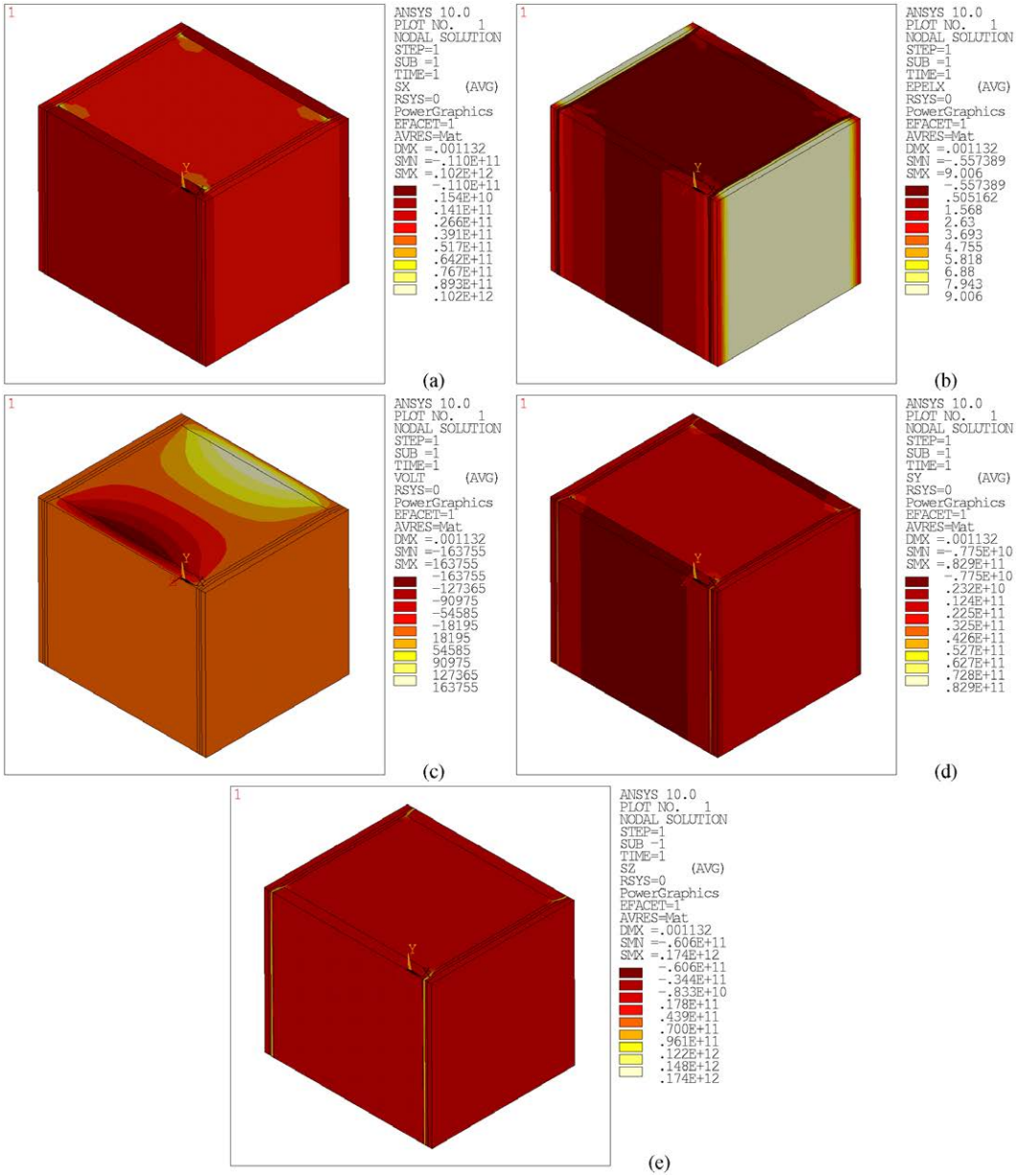

Figure 18. Distributions induced by a unitary normal strain $S_1 = (u_1^{X_1^+} - u_1^{X_1^-})/h_T = 1$ (problem 1) applied to the d_{15} MFC RVE: (a) normal stress T_1, (b) normal strain S_1, (c) electric potential, (d) normal stress T_2 and (e) normal stress T_3.

homogenization method considered for the active layer could be also applied to the seven-layered d_{15} MFC. In this case, however, in addition to relative mechanical displacement and electric voltage boundary conditions applied on the boundaries of the RVE (X_1^-, X_1^+, X_2^-, X_2^+, X_3^-, X_3^+), electric voltage boundary conditions are also imposed at the electrodes on surfaces X_1^{e-} and X_1^{e+}. In the case of the RVE considered for the d_{15} MFC, shown in figure 16, these boundaries are X_1^-: $x_1 = 0$, X_1^+: $x_1 = h_T = h_P + 2(h_E + h_A + h_K)$, X_2^-: $x_2 = 0$, X_2^+: $x_2 = w$, X_3^-: $x_3 = 0$, X_3^+: $x_3 = L_P + L_E$, X_1^{e-}: $x_1 = h_E + h_A + h_K$, X_1^{e+}: $x_1 = h_P + h_E + h_A + h_K$.

Notice that the isotropy of the electrode layer depends on its design, which remains an open issue. Electrode designs such as those used for the d_{31} MFC (continuous) seem to be more reasonable than those used for the d_{33} MFC (interdigitated) since the voltage should ideally be constant all over the electrode surface. However, since only the piezoelectric fibres must be covered with top and bottom electrodes, different designs can be considered to enhance their properties and thus the d_{15} MFC effective properties. Evidently, the isotropy assumed in this work is only a first approximation since the optimal electrode design for the d_{15} MFC is not yet defined. Future works should account for this aspect.

Figure 17 shows the finite element mesh used in Ansys® for the seven-layered d_{15} MFC RVE using an FVF of 0.86 for the PZT + epoxy active layer. The 3D 20-node coupled-field solid finite element SOLID226 was used to mesh all volumes. 5525 finite elements were used considering 25 divisions in the x_1 direction (13 divisions for the PZT layer and two divisions

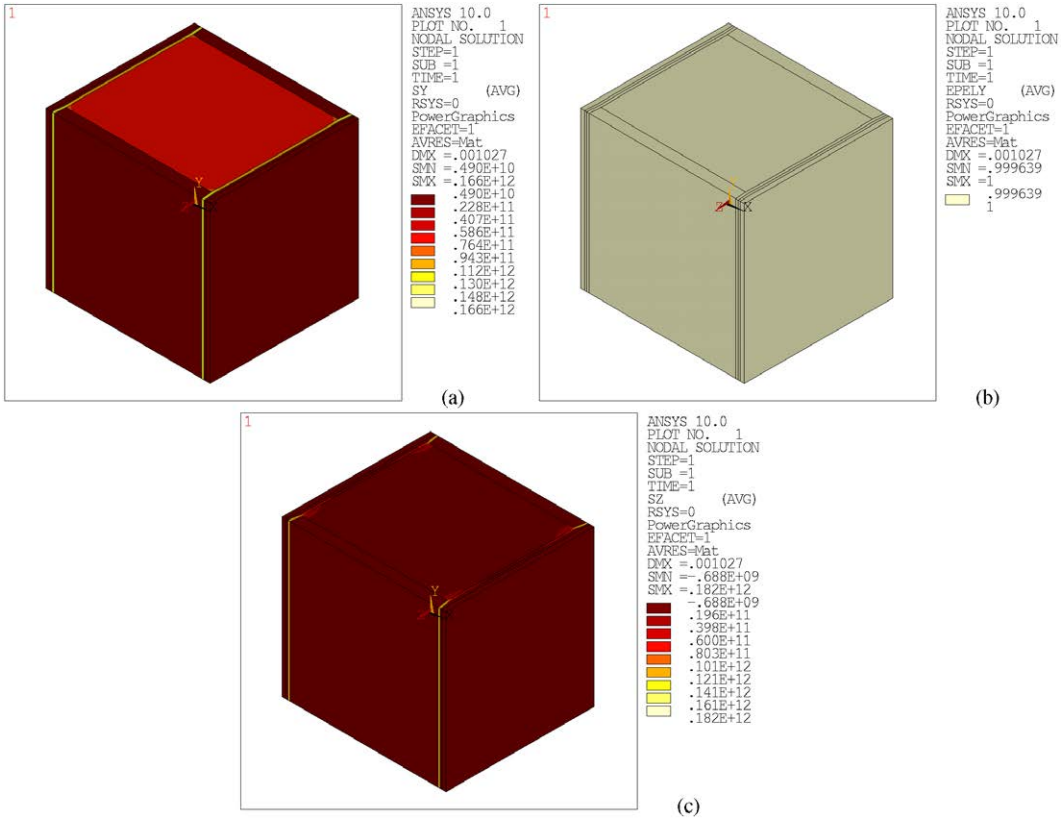

Figure 19. Distributions induced by a unitary normal strain $S_2 = (u_2^{X_2^+} - u_2^{X_2^-})/w = 1$ (problem 2) applied to the d_{15} MFC RVE: (a) normal stress T_2, (b) normal strain S_2 and (c) normal stress T_3.

for each electrode and protective layer), 13 divisions in the x_2 direction and 17 divisions in the x_3 direction (11 divisions for the PZT layer and three divisions for each epoxy layer). According to figure 16, the dimensions considered for this RVE are $h_P = 1$ mm, $h_K = 25.4$ μm, $h_A = 12.7$ μm, $h_E = 17.8$ μm, $L_P = 0.860$ mm, $L_E = 0.140$ mm and $w = 1$ mm [4]. The material properties for the active layer (Sonox-P502 and epoxy) are those considered in section 4. The materials properties for the protective layers, taken from [4], are Kapton: $Y = 2.5$ GPa, $\nu = 0.34$ and $\epsilon = 3.4\epsilon_0$; and acrylic: $Y = 2.7$ GPa, $\nu = 0.35$ and $\epsilon = 3.4\epsilon_0$. The electrode layer, made of copper and epoxy, is considered to be isotropic and its properties are found by a linear mixture considering an 80% copper volume fraction, leading to $Y = 90$ GPa, $\nu = 0.3$ and $\epsilon = 4.25\epsilon_0$.

The distributions of normal and shear stresses and strains for the local problems used to evaluate the effective elastic properties of the seven-layered d_{15} MFC RVE using an FVF of 0.86 for the PZT + epoxy active layer are presented in figures 18–23. As can be noticed from figure 18(b), unlike the previous case, the now present softer protective layers concentrate the S_1 normal strains. Hence, only for the S_2 normal strains (normal to the shear plane of interest), are the strains homogeneous (figure 19(b)). Notice also from figure 19(a) that the two electrode layers (copper + epoxy) are relatively stiff (compared to piezoceramic fibre and epoxy and protective Kapton and acrylic layers) and thus present high stress values. In problem 3, the strain is still concentrated in the epoxy layer but is no longer layerwise homogeneous due to the electrode and protective layers (figure 20(b)). The electrode layers' relatively high stiffness is also responsible for a smoother transition between the shear strains, S_4 and S_5, from the piezoceramic fibre and epoxy layer (figures 21(b) and 22(b)). The S_6 shear strain is no longer homogeneous and is concentrated in the protective layers (figure 23(b)). It can also be noticed that the electrode and protective layers lead to an overall increase in the non-homogeneous distributions of mechanical and electrical quantities.

The distributions of shear strain S_5, electric displacement D_1 and electric field E_1 for the local problem used to evaluate the effective piezoelectric and dielectric properties, d_{15} and ϵ_{11}^T, of the seven-layered d_{15} MFC RVE using an FVF of 0.86 for the PZT + epoxy active layer are presented in figure 24. It can be noticed that the shear strain is concentrated in the piezoceramic fibre while the other layers just follow the deformation imposed by the piezoceramic fibre (figure 24(a)). Figure 24(b) shows that the electric displacement is also concentrated in the piezoceramic material. However, as in the previous case (figure 15(c)), the electric field is homogeneous in the piezoceramic fibre and epoxy layers since it is assumed that the electrode entirely covers the active layer (figure 24(c)).

Table 5 shows the effective properties, transformed to Voigt notation, of the seven-layered d_{15} MFC using FVFs of 0.86 and 0.95 for the PZT + epoxy active layer obtained by the finite element local problems. Comparison of table 5 with Tables 3 and 4 shows that, while the active layer is transversally

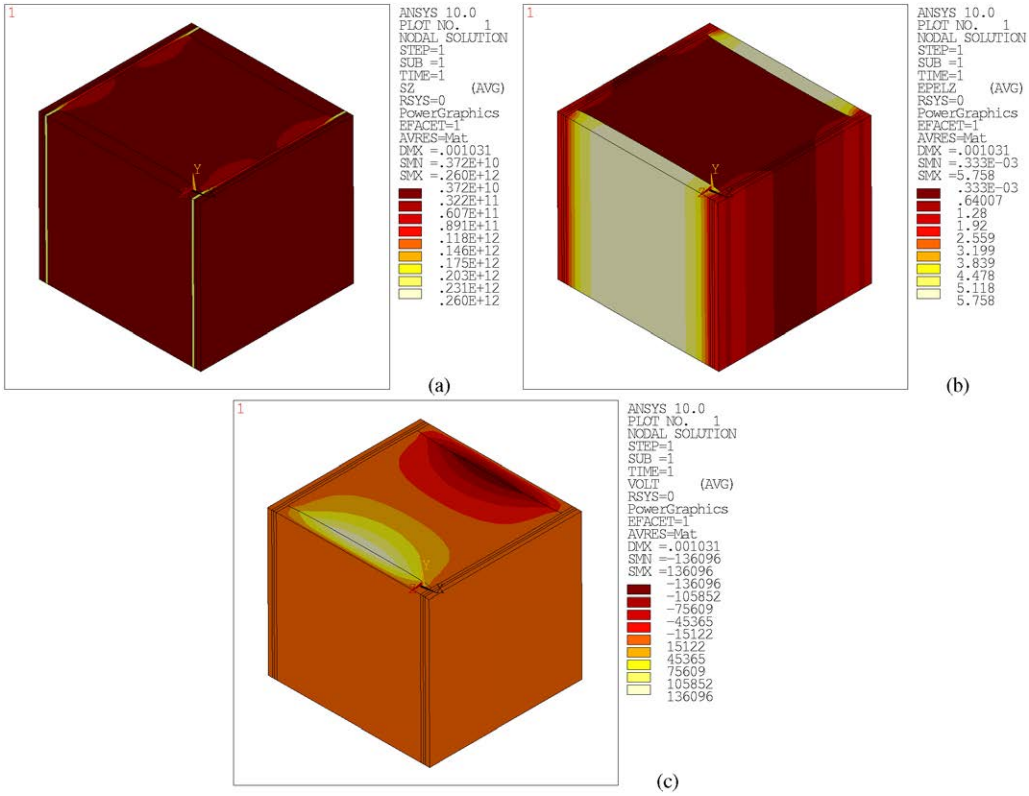

Figure 20. Distributions induced by a unitary normal strain $S_3 = (u_3^{X_3^+} - u_3^{X_3^-})/(L_P + L_E) = 1$ (problem 3) applied to the d_{15} MFC RVE: (a) normal stress T_3, (b) normal strain S_3 and (c) electric potential.

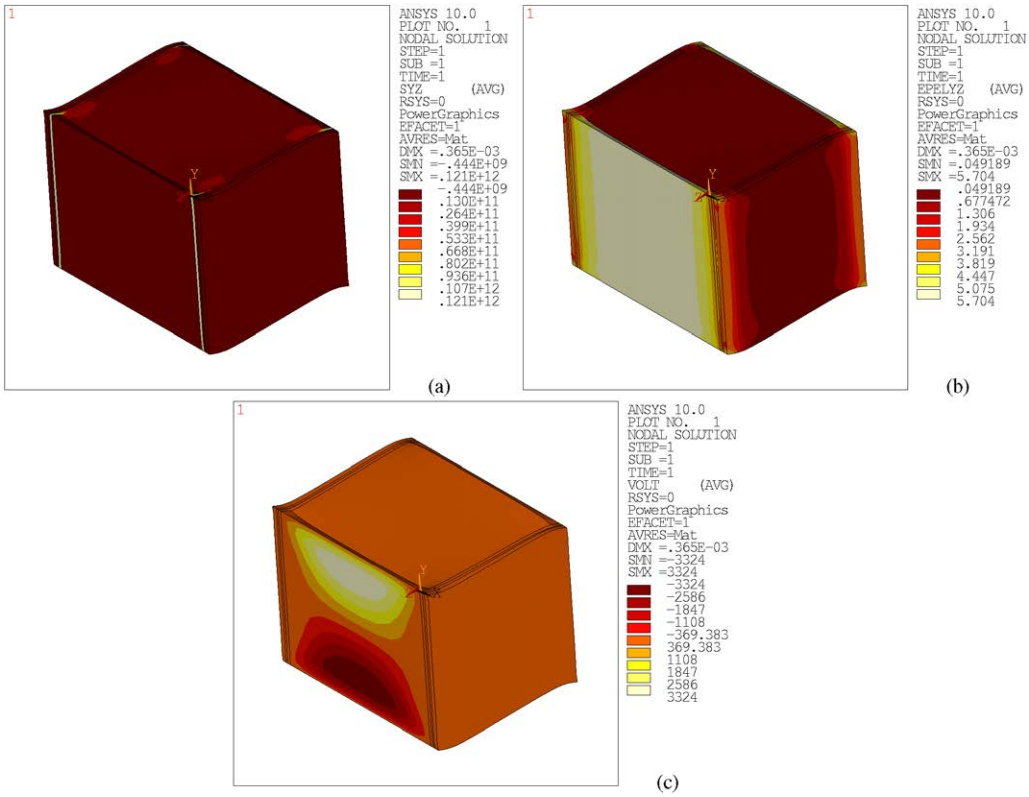

Figure 21. Distributions induced by a unitary shear strain $S_4 = 1$ (problem 4) applied to the d_{15} MFC RVE: (a) shear stress T_4, (b) shear strain S_4 and (c) electric potential.

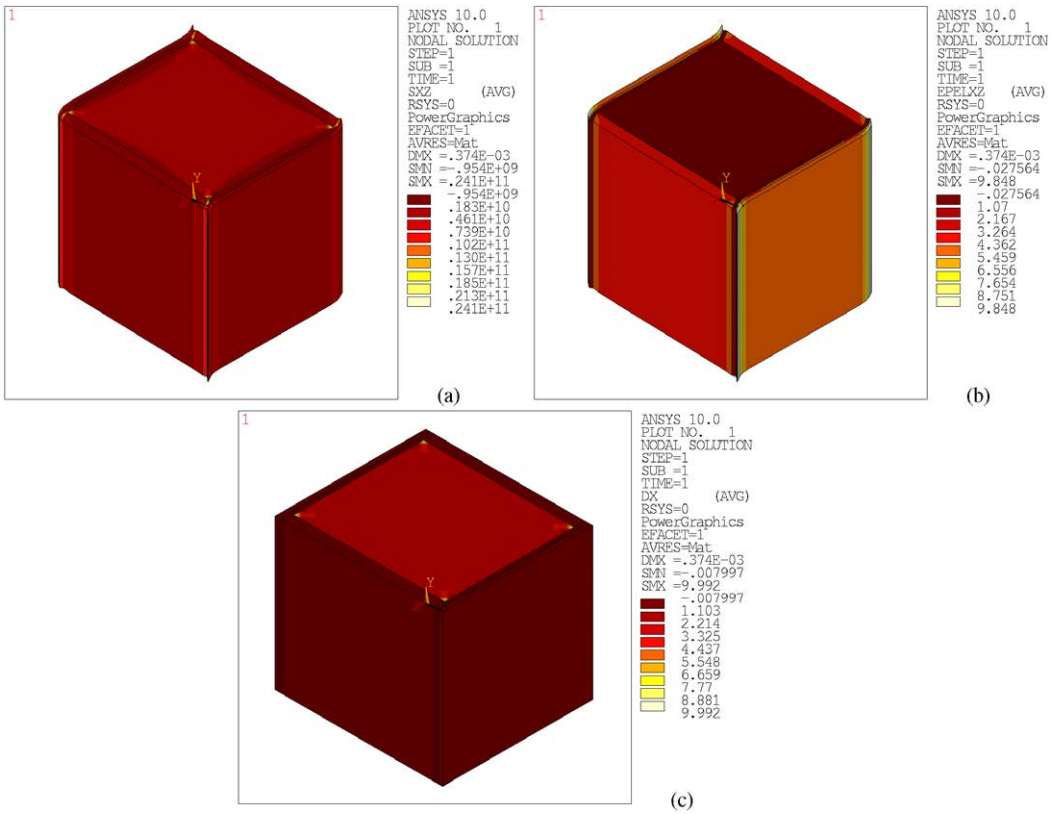

Figure 22. Distributions induced by a unitary shear strain $S_5 = 1$ (problem 5) applied to the d_{15} MFC RVE: (a) shear stress T_5, (b) shear strain S_5 and (c) electric displacement D_1.

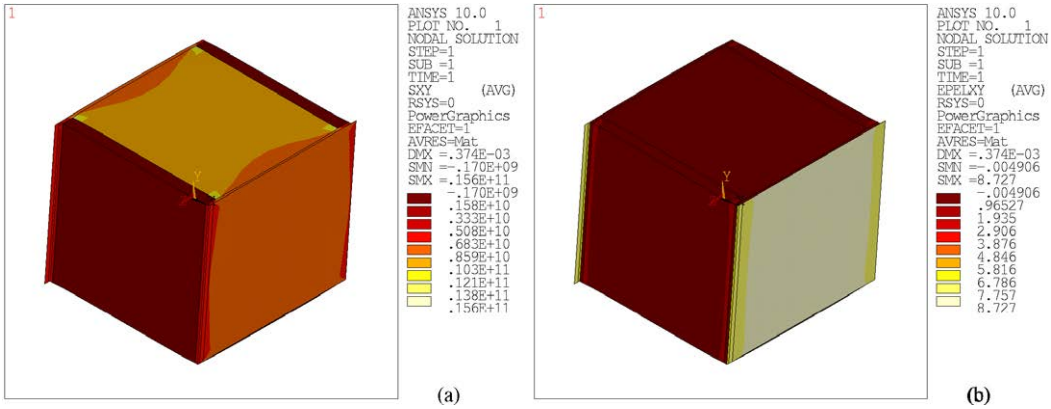

Figure 23. Distributions induced by a unitary shear strain $S_6 = 1$ (problem 6) applied to the d_{15} MFC RVE: (a) shear stress T_6 and (b) shear strain S_6.

isotropic, the seven-layered composite is orthotropic. In particular, the Young modulus Y_1 is significantly diminished due to the relatively soft protective layers. On the other hand, the Young modulus Y_3 is increased mainly due to the electrode that is stiffer than the epoxy core and thus promotes a stiffer connection between the X_3^+ surface and the PZT core. The shear modulus G_{13} is diminished by 23% due to the protective layers which are softer than the PZT. Notice, however, that the thickness of the protective and electrode layers should also play a major role in this shear modulus. For instance, thinner protective layers should increase the shear modulus G_{13}, but they would also perform poorly as protective layers. The piezoelectric constant d_{15} is increased a little while e_{15} is decreased by 30%, from 3.13 to 2.20 C m^{-2}. The dielectric constant ϵ_{11}^T is not modified due to the protective and electrode layers since it is assumed that the electric contact between the electrode and the PZT occurs at the PZT–electrode interface. This would not be the case if there was an epoxy layer between the copper electrode and the PZT. These effective properties yield an overall smaller electromechanical coupling coefficient k_{15}, such that the efficiency in energy conversion k_{15}^2 decreases by 20%, from 10% to 8%. Notice that this is much less than the k_{15}^2 of the PZT (Sonox-P502) alone of 54.8%.

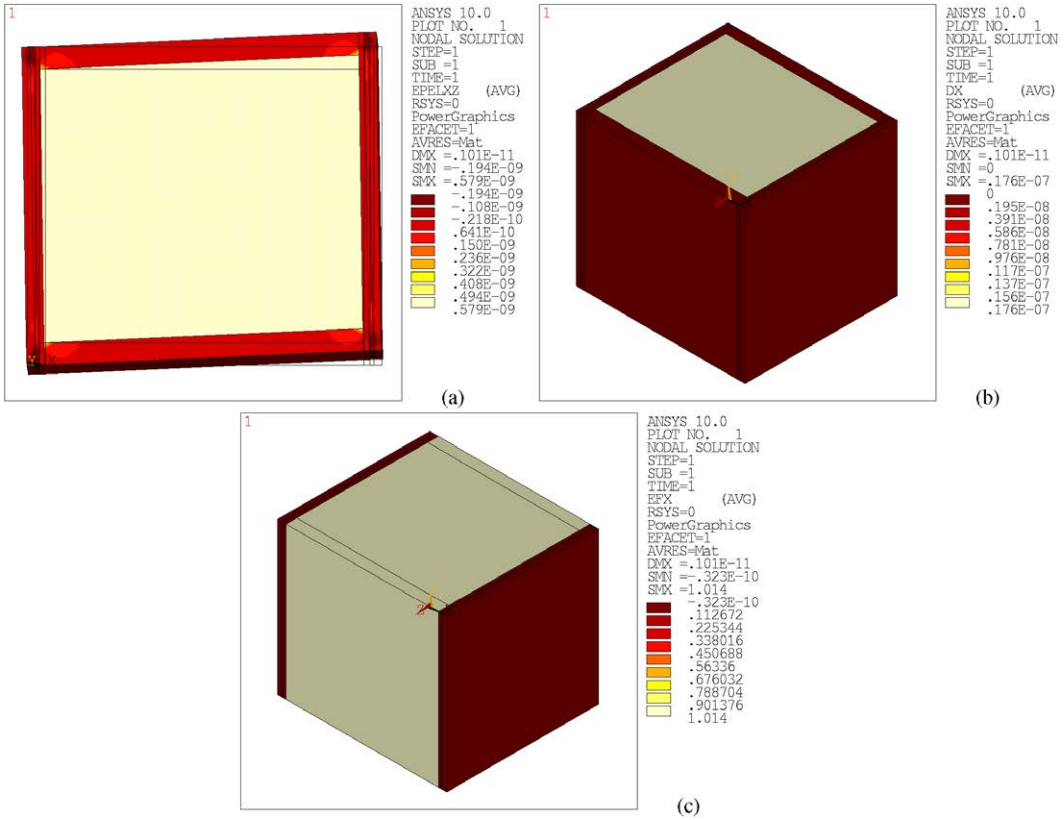

Figure 24. Distributions induced by a unitary electric field $E_1 = (\phi^{X_1^{e+}} - \phi^{X_1^{e-}})/h_P = 1$ applied to the d_{15} MFC RVE: (a) shear strain S_5, (b) electric displacement D_1 and (c) electric field E_1.

Table 5. Effective short circuit elastic and piezoelectric properties of the d_{15} MFC with electrode and protective layers (seven layers).

FVF = 0.86	FVF = 0.95
$Y_1 = 26.72$ GPa	$Y_1 = 28.84$ GPa
$Y_2 = 48.16$ GPa	$Y_2 = 52.37$ GPa
$Y_3 = 23.63$ GPa	$Y_3 = 37.56$ GPa
$G_{23} = 9.04$ GPa	$G_{23} = 14.85$ GPa
$G_{13} = 4.99$ GPa	$G_{13} = 7.37$ GPa
$G_{12} = 7.80$ GPa	$G_{12} = 8.18$ GPa
$\nu_{12} = 0.24$	$\nu_{12} = 0.23$
$\nu_{13} = 0.17$	$\nu_{13} = 0.14$
$\nu_{23} = 0.24$	$\nu_{23} = 0.23$
$d_{15} = 484.80$ pC N^{-1}	$d_{15} = 533.12$ pC N^{-1}
$e_{15} = 2.20$ C m^{-2}	$e_{15} = 3.56$ C m^{-2}
$\epsilon_{11}^T = 14.85$ nF m^{-1}	$\epsilon_{11}^T = 16.40$ nF m^{-1}
$k_{15}^2 = 7.9\%$	$k_{15}^2 = 12.8\%$
$k_{15} = 28\%$	$k_{15} = 36\%$

6. Concluding remarks

In the present work, a finite element homogenization method for a shear actuated d_{15} macro-fibre composite (MFC) made of seven layers (Kapton, acrylic, electrode, piezoceramic fibre and epoxy composite, electrode, acrylic, Kapton) was proposed and used for the characterization and identification of its effective material properties. The methodology was first validated for the MFC active layer only, made of the piezoceramic fibre and epoxy, through comparison with previously published analytical results. Then, the methodology was applied to the full MFC with seven layers. It was shown that the packaging reduces significantly the shear stiffness of the piezoceramic material and, thus, leads to significantly smaller effective electromechanical coupling coefficient k_{15} and piezoelectric stress constant e_{15} when compared to the piezoceramic fibre properties. However, the piezoelectric charge constant d_{15} was less affected by the softer layers required by the MFC packaging. This might indicate that this MFC design could be interesting for sensing applications but not so much for actuation. The presented results also confirmed that a higher fibre volume fraction (FVF) is desirable and a 95% FVF seems to be a good compromise.

Future works will be directed to parametric analyses aiming at the optimization of elastic, piezoelectric and dielectric properties of shear actuated d_{15} MFCs. Some parameters already seem to be good candidates to affect the electromechanical coupling performance of such transducers, such as the relative thickness of the active layer and the protective and electrode layers, the electrode layer stiffness yielded by the electrode design and, of course, the fibre volume fraction of the active layer.

Acknowledgments

The authors acknowledge the support of the MCT/CNPq/FAPEMIG National Institute of Science and Technology on Smart Structures in Engineering, grant no. 574001/2008-5.

References

[1] Skinner D P, Newnham R E and Cross L E 1978 Flexible composite transducers *Mater. Res. Bull.* **13** 599–607

[2] Wilkie W K, Bryant G R, High J W, Fox R L, Hellbaum R F, Jalink A, Little B D and Mirick P H 2000 Low-cost piezocomposite actuator for structural control applications *Smart Structures and Materials: 2000 Industrial and Commercial Applications of Smart Structures Technologies* (*Proc. SPIE* vol 3991) ed J H Jacobs (Bellingham, WA: SPIE Optical Engineering Press) pp 323–34 *(Newport Beach, March)*

[3] Bent A A and Hagood N W 1997 Piezoelectric fiber composites with interdigitated electrodes *J. Intell. Mater. Syst. Struct.* **8** 903–19

[4] Raja S and Ikeda T 2008 Concept and electro-elastic modeling of shear actuated fiber composite using micro-mechanics approach *J. Intell. Mater. Syst. Struct.* **19** 1173–83

[5] Sun C T and Zhang X D 1995 Use of thickness-shear mode in adaptive sandwich structures *Smart Mater. Struct.* **4** 202–6

[6] Benjeddou A, Trindade M A and Ohayon R 1997 A unified beam finite element model for extension and shear piezoelectric actuation mechanisms *J. Intell. Mater. Syst. Struct.* **8** 1012–25

[7] Benjeddou A 2007 Shear-mode piezoceramic advanced materials and structures: a state of the art *Mech. Adv. Mater. Struct.* **14** 263–75

[8] Trindade M A and Benjeddou A 2009 Effective electromechanical coupling coefficients of piezoelectric adaptive structures: critical evaluation and optimization *Mech. Adv. Mater. Struct.* **16** 210–23

[9] Benjeddou A, Trindade M A and Ohayon R 2000 Piezoelectric actuation mechanisms for intelligent sandwich structures *Smart Mater. Struct.* **9** 328–35

[10] Raja S, Prathap G and Sinha P K 2002 Active vibration control of composite sandwich beams with piezoelectric extension-bending and shear actuators *Smart Mater. Struct.* **11** 63–71

[11] Baillargeon B P and Vel S S 2005 Exact solution for the vibration and active damping of composite plates with piezoelectric shear actuators *J. Sound Vib.* **282** 781–804

[12] Benjeddou A and Ranger J-A 2006 Use of shunted shear-mode piezoceramics for structural vibration passive damping *Comput. Struct.* **84** 1415–25

[13] Trindade M A and Maio C E B 2008 Multimodal passive vibration control of sandwich beams with shunted shear piezoelectric materials *Smart Mater. Struct.* **17** 055015

[14] Deraemaeker A, Nasser H, Benjeddou A and Preumont A 2009 Mixing rules for the piezoelectric properties of macro fiber composites *J. Intell. Mater. Syst. Struct.* **20** 1475–82

[15] Deraemaeker A and Nasser H 2010 Numerical evaluation of the equivalent properties of macro fiber composite (MFC) transducers using periodic homogenization *Int. J. Solids Struct.* **47** 3272–85

[16] Biscani F, Nasser H, Belouettar S and Carrera E 2011 Equivalent electro-elastic properties of macro fiber composite (MFC) transducers using asymptotic expansion approach *Composites* B **42** 444–55

[17] Benjeddou A and Al-Ajmi M 2011 Analytical homogenizations of piezoceramic shear macro-fibre composites *Proc. IUTAM Symposium on Multiscale Modelling of Fatigue, Damage and Fracture in Smart Materials Systems* ed M Kuna and A Ricoeur (Dordrecht: Springer) pp 229–42

[18] Otero J A, Rodriguez-Ramos R, Monsivais G and Perez-Alvarez R 2005 Dynamical behavior of a layered piezocomposite using the asymptotic homogenization method *Mech. Mater.* **37** 33–44

[19] Berger H, Kari S, Gabbert U, Rodriguez-Ramos R, Guinovart R, Otero J A and Bravo-Castirello J 2005 An analytical and numerical approach for calculating effective material coefficients of piezoelectric fiber composites *Int. J. Solids Struct.* **42** 5692–714

[20] Trindade M A and Benjeddou A 2010 Modelling and characterization of shear actuated piezoelectric fibre composites, Valencia *Proc. 10th Int. Conf. on Computational Structures Technology* ed B H V Topping *et al* (Stirlingshire: Civil-Comp Press) p 69

[21] Ikeda T 1990 *Fundamentals of Piezoelectricity* (Oxford: Oxford University Press)

[22] APC International 2010 *Physical and Piezoelectric Properties of APC Materials* www.americanpiezo.com/apc-materials/piezoelectric-properties.html Accessed 19 March 2010

[23] ITT Corporation 2009 *Electro-ceramic Products and Material Specification* http://uss.es.itt.com/as/docs/ITTElecCeramProdMatSpecJune09.pdf accessed 19 March 2010

[24] PI Ceramic 2010 *Typical Parameters of Piezoelectric Ceramics* www.piceramic.com/piezo_materials_2.php accessed 19 March 2010

[25] Morgan Electro Ceramics 2008 *Piezoelectric Ceramics* www.morganelectroceramics.com/materials/piezoelectric/ accessed 19 March 2010

[26] CeramTec GmbH Multifunctional Ceramics Division 2008 *Materials for Sensors* www.ceramtec.com/downloads/mf_materials-sensors.pdf accessed 5 March 2010

[27] Deraemaeker A, Benelechi S, Benjeddou A and Preumont A 2007 Analytical and numerical computation of homogenized properties of MFCs: application to a composite boom with MFC actuators and sensors *Proc. III ECCOMAS Thematic Conf. on Smart Structures and Materials (Gdansk, July 9–11)* ed W Ostachowicz, J Holnicki-Szulc and C A Mota Soares